ISSN 1068-3755, Surface Engineering and Applied Electrochemistry, 2022, Vol. 58, No. 4, pp. 369–385. © Allerton Press, Inc., 2022.
Russian Text © The Author(s), 2021, published in Elektronnaya Obrabotka Materialov, 2021, No. 5, pp. 34–51.

Characteristics and Plasma Parameters of the Overstressed Nanosecond Discharge in Air between an Aluminum Electrode and a Chalcopyrite Electrode ($CuInSe_2$)

A. K. Shuaibov[a], *, A. I. Minya[a], A. A. Malinina[a], R. V. Gritsak[a], A. N. Malinin[a], Yu. Yu. Bilak[a], and M. I. Vatrala[a]

[a] *Uzhhorod National University, Uzhhorod, 88000 Ukraine*

**e-mail: alexsander.shuaibov@uzhnu.edu.ua*

Received November 26, 2020; revised March 15, 2021; accepted March 17, 2021

Abstract—The characteristics and parameters of an overstressed high-current discharge with a duration of 100–150 ns in air, which was ignited between an aluminum electrode and a chalcopyrite electrode ($CuInSe_2$), are presented. The air pressure was 13.3 and 101.3 kPa. In the process of microexplosions of inhomogeneities on the working surfaces of electrodes in a strong electric field, aluminum vapors and chalcopyrite vapors were introduced into the interelectrode gap, which creates the prerequisites for the synthesis of thin films based on quaternary chalcopyrite: $CuAlInSe_2$. The films synthesized from the products of electrode destruction were deposited on a quartz plate at a distance of 2–3 cm from the center of the discharge gap. The current and voltage pulses across the discharge gap of $d = 1$ mm, as well as the pulse energy input into the discharge, were investigated. The plasma emission spectra were studied, which made it possible to establish the main decay products of the chalcopyrite molecule and the energy states of atoms and singly charged ions of aluminum, copper and indium, which are formed in the discharge. The reference spectral lines of atoms and ions of aluminum, copper, and indium were established, which can be used to control the process of deposition of thin films of quaternary chalcopyrite. Thin films were synthesized from the degradation products of chalcopyrite molecules and aluminum vapors, which may have the composition of the quaternary chalcopyrite $CuAlInSe_2$; the transmission spectra of the synthesized films in the spectral range of 200–800 nm were studied. By the method of numerical simulation of the plasma parameters of an overstressed nanosecond discharge based on aluminum and chalcopyrite vapors in air by solving the Boltzmann kinetic equation for the electron energy distribution function, the electron temperature and density, the specific power losses of the discharge for the main electronic processes and their rate constants depending on the value parameter E/N for plasma of vapor-gas mixtures based on air, aluminum vapor, and ternary chalcopyrite were modulated.

Keywords: overstressed nanosecond discharge, chalcopyrite, aluminum, air, plasma parameters

DOI: 10.3103/S1068375522040123

INTRODUCTION

The optical characteristics of plasma of overstressed discharges in gases of nano- and subnanosecond duration are primarily characterized by the spectral lines of atoms and ions of the electrode material [1–4]. For example, it was found that the emission spectra of the near-cathode plasma nanosecond discharge in air exhibit the continuum of the band of the second positive system of the nitrogen molecule, characteristic of spark discharges, the spectral lines N(I), N(II), H(I) and lines of the cathode material [1]. The temperature of such a plasma was in the range of 0.5–1.8 eV, and the electron density reached 2×10^{17} cm^{-3}.

The results of later studies of the emission characteristics of overstressed nanosecond discharge between metal or chalcopyrite electrodes are given in [2–4]. The resulting emission spectra were determined by lines on the transitions of atoms and singly charged ions of copper, zinc, aluminum, and iron, as well as lines of atoms, singly charged atomic ions of nitrogen and bands of the nitrogen molecule.

It follows from the results of studying the characteristics of an overstressed nanosecond discharge initiated by a beam of runaway electrons in nitrogen [5] that colored minijets of aluminum vapor plasma are formed near the cathode tip. The duration of luminescence at Al(I) and Al(II) transitions exceeded 2 μs, which is longer than the duration of current pulses. Therefore, the authors of [5] proposed a recombination mechanism for populating the upper excited levels of Al(I) and Al(II) in this discharge. At $p(N_2) = 13.3$ kPa, the discharge contraction occurred when voltage pulses reflected from plasma reappeared in the discharge gap due to a mismatch between the load resis-

tance and the output resistance of the high-voltage modulator of nanosecond voltage pulses.

The optical characteristics of a laser plasma in air, which was formed using Nd:YAG laser radiation with a radiation power density on the target surface of 6.4–38.4 J/cm^2 were given in [6]. It is of interest to compare the optical characteristics of the laser plasma with the corresponding results for an overstressed nanosecond discharge in air between aluminum and iron electrodes. In contrast to the discharge plasma, which is close in terms of the initiation conditions to the laser air plasma with aluminum and iron targets, no ion spectral lines were observed.

The results of studying gas-dynamic processes in an overstressed nanosecond discharge in air (p = 101 kPa) [7] were obtained by visualization using a laser monitor and shadow image analysis techniques. It is shown that metal vapors are formed in such a discharge, which, in a time of ≈1 μs, enter the space between the electrodes, where they are excited and ionized. Some of these vapors, together with plasma products, are carried out in the radial direction for a time of ≈2.5 ms under the effect of gas-dynamic processes and are deposited on the walls of the discharge chamber in the form of nanostructured films.

The shadow photography method has also been successfully used to study the very nature of the overstressed spark discharge in gases. The frames of glow and shadow-grams of plasma of the initial stages of spark and diffuse nanosecond discharges in the needle-plane interval were obtained in [8]. It is possible to distinguish the following stages of such a discharge in plasma photographs: the formation of a diffuse channel and cathode spots on the surface of a flat electrode in the time interval τ = 0–5 ns; the formation of thin plasma channels that developed from the needle electrode and closed on the cathode spots at τ = 5–10 ns, and a spark channel was formed after that.

The authors of [9] assume that preionization of the gas in front of the streamer is carried out by fast electrons with an energy of 0.1–10 keV for pulses of the negative polarity on a needle electrode, while that for voltage pulses of the positive polarity is by quanta of characteristic X-ray radiation.

In addition to the aluminum plasma, vapors of other electrode materials were successfully introduced into the discharge gap of overstressed nanosecond discharges. The optical characteristics of copper and iron plasmas are given in [10]. Blue plasma jets were generated by a discharge in nitrogen ($p(N_2)$ = 100–200 Torr), when the cathode was made of stainless steel. For a copper cathode ($p(N_2)$ = 30–59 Torr), green plasma jets were generated. They came from bright spots on the working surface of the needle cathode. For discharges with an aluminum cathode, the plasma jets were blue. The appearance of these plasma jets is associated with microexplosions of natural inhomogeneities on the cathode surface and electroerosion of the metal, resulting in ectons and vapors of the cathode material.

The spectral characteristics of an overstressed pulsed discharge with a duration of 2.5 ns are given in [11]. The most intense groups of copper lines in its emission spectra from the region near the copper tip of the cathode were observed in the spectral intervals of 190–230 and 300–350 nm and CN(B–X) radical bands. In this case, no continuum was observed in the spectra. As the nitrogen pressure increases from 100 to 760 Torr, the intensity of the copper lines in the wavelength range of 190–230 and 300–350 nm increased. The duration of the emission of the 521.8 nm Cu(1) spectral line on the emission waveform from the discharge zone near the needle tip was 1 μs. It significantly exceeded the duration of the current pulses (τ = 2.5 ns), which may be associated with the energy transfer from nitrogen molecules in the metastable state ($N_2(A^3\Sigma_u^+)$) to copper atoms ($Cu(1)(^2D_{5/2})$).

Since the conditions for ignition of the diffuse stage of the overstressed nanosecond discharge in a nonuniform electric field are of great importance for practical applications, determining the condition for generating a beam of runaway electrons and the accompanying X-ray radiation in high-pressure gases, especially for submicrosecond voltage pulses, continues to be relevant. For example, the main features of the generation of a beam of runaway electrons in air were considered in [12] for a duration of the leading edge of a voltage pulse of 500 ns. It was shown [12] that a beam of runaway electrons is generated at the voltage pulse amplitude of ≥100 kV and high average electric field strength. In this case, the closing of the discharge gap by the streamer creates an electric field near the cathode that is sufficient for the occurrence of field emission, which causes the transformation of the streamer channel into a spark one. The space charge of the streamer creates a field sufficient for field emission at typical breakdown voltages [13].

Since it is important to establish a relationship between the plasma discharge parameters and the characteristics of the synthesized nanostructures when synthesizing nanostructures in a high-voltage nanosecond discharge, modern methods of plasma diagnostics acquire an important role. The parameters of air and nitrogen plasma (at p = 101 kPa) obtained using an electric generator with a power of 50 kW at f = 4 MHz, are given in [14]. The electron density of such a plasma was ≈5 × 10^{13} cm^{-3}, and the concentration of molecular nitrogen ions was ≈7 × 10^{10} cm^{-3}.

The results of studying the destruction of metal alloys and thin wires in the plasma of a high-voltage nanosecond discharge are presented in [15]. The characteristics of the synthesized nanostructures of lead, tin, bismuth, tungsten, and molybdenum oxides and nanowhiskers of tin–lead, bismuth–lead–tin, and molybdenum oxides, which have the properties of thermistors and thermoelectrics, are presented.

Synthesis conditions and characteristics of synthesized silicon nanoparticles 3–5 nm in diameter in a repetitively pulsed discharge in argon are presented in [16]. The studies were carried out at an interelectrode distance of 2 mm, pulse repetition rate of 100–300 Hz, their duration of 0.2–5 μs, voltage pulse amplitude of 3–14 kV, and current pulse amplitude of 12–350 A.

In [17], it was reported on the fabrication of a $CuIn_{1-x}Al_xSe_2$ (CIASe) thin-film solar cell based on selenization of metal precursors. The best solar cells based on CIASe have a coefficient of performance (COP) of 6.5% with an optimal aluminum content in quaternary chalcopyrite Al/(In + Al) of 0.2. A comparison of these values with similar values for a solar cell made without aluminum showed a significant increase in the efficiency of the device due to an increase in the band gap in the quaternary chalcopyrite $CuIn_{1-x}Al_xSe_2$. "Already existing commercial elements on a different basis have an efficiency of up to 20–22%. Therefore, at present, for practical applications it is important to search for new, cheaper plasma methods for synthesizing films for photovoltaic devices, including solar cells based on films of complex chalcopyrites."

This work presents the results of studying the characteristics of the overstressed, nanosecond discharge between an aluminum electrode and an electrode of ternary chalcopyrite ($CuInSe_2$) in air; on the basis of electrode sputtering products, thin films were synthesized from vapors of ternary chalcopyrite and products of its destruction in plasma and aluminum vapors, and their transmission spectra are studied; the results of plasma parameter simulation by solving the Boltzmann kinetic equation for the electron energy distribution function are presented, which made it possible to determine the temperature and drift velocity of plasma electrons, the specific energy losses for the main electronic processes, and the rate constants of the main electronic processes in the plasma under study.

EXPERIMENTAL TECHNIQUE AND ELECTRICAL CHARACTERISTICS

A nanosecond, high-current discharge between an aluminum electrode and a ternary chalcopyrite ($CuInSe_2$) electrode was ignited in a sealed dielectric chamber. The scheme of the discharge module and device for the deposition of thin films is given in [2–4]. The distance between the electrodes was 1 mm, which provided overvoltage of the discharge gap at air pressures of 13.3 and 101.3 kPa. The diameter of the cylindrical electrodes was 5 mm, and the curvature radius of their working end surface was 3 mm. The discharge ignition was carried out using a bipolar high-voltage voltage pulse modulator from a total pulse duration of 50–100 ns with an amplitude of positive and negative components of ±20–40 kV. The pulse repetition rate was 100 Hz, since a strong heating of the discharge device was observed at high frequencies. Voltage pulse waveforms across the discharge gap and current pulse waveforms were recorded using a broadband capacitive voltage divider, a Rogowski coil, and a 6LOR-04 broadband oscilloscope with a time resolution of 2–3 ns.

Plasma emission pulses at the transitions of individual spectral lines were recorded using an electron linear multiplier (ELU-14-FS) and a 6LOR high-speed six-channel oscilloscope. The time resolution of this block of the recording system was 1–2 ns. The voltage waveforms on the electrodes of the discharge device were recorded using a low-inductance voltage divider with a time resolution of 2–3 ns, and current pulse waveforms were recorded using a Rogowski coil, which had a time resolution of 20–30 ns.

The results of control experiments on studying the characteristics of overstressed nanosecond discharge at different air pressures in systems, when two identical electrodes made of aluminum [4] or ternary chalcopyrite were used, are given in [2, 18]. In both cases, the interelectrode distance was 1 mm and the discharge was visually spatially homogeneous, which is associated with the possibility of preionization of the gaseous medium from the beam of runaway electrons and the accompanying X-ray radiation [19]. The plasma discharge volume depended on the frequency of the voltage pulses. The "point discharge" mode was achieved only at voltage pulse repetition rates in the range of $f = 40–150$ Hz. At a short-term increase in frequency to 1000 Hz, the plasma volume of the gas-discharge emitter increased to 100 mm^3.

The characteristic voltage and current pulse waveforms in discharges between two aluminum and chalcopyrite electrodes are given in [4, 20, 21] at atmospheric air pressure. Voltage and current waveforms were in the form of oscillations damped in time with a duration of ≈10 ns, which is caused by a mismatch between the output resistance of the high-voltage modulator and the load resistance: plasma. When the distance between the electrodes increases from 1 to 5 mm, matching of the resistances improves, and the number of oscillations in the voltage and current pulses decreases. But such a regime was not optimal for the formation of plasma flows based on the electrode material as well as for a high-voltage discharge of nanosecond duration between aluminum electrodes [6].

Figures 1 and 2 show voltage and current waveforms and pulse power of the overstressed nanosecond discharge between aluminum electrode and chalcopyrite electrode at air pressures of 13.3 and 101.3 kPa.

At an air pressure of 13.3 kPa (Fig. 1), the largest mismatch was observed between the output resistance of the generator of high-voltage voltage pulses and the load resistance: the overstressed nanosecond discharge plasma. The total duration of voltage and current oscillations across the discharge gap reached 450 ns, while the duration of individual voltage oscillations was 7–10 ns, and the duration of current oscil-

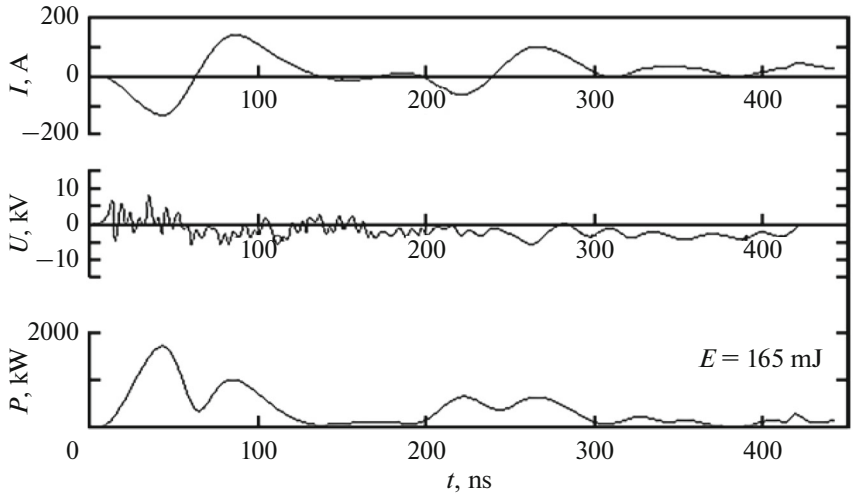

Fig. 1. Current, voltage, and pulsed power waveforms of the overstressed bipolar nanosecond discharge between electrodes of aluminum and chalcopyrite ($CuInSe_2$) at the air pressure of 13.3 kPa.

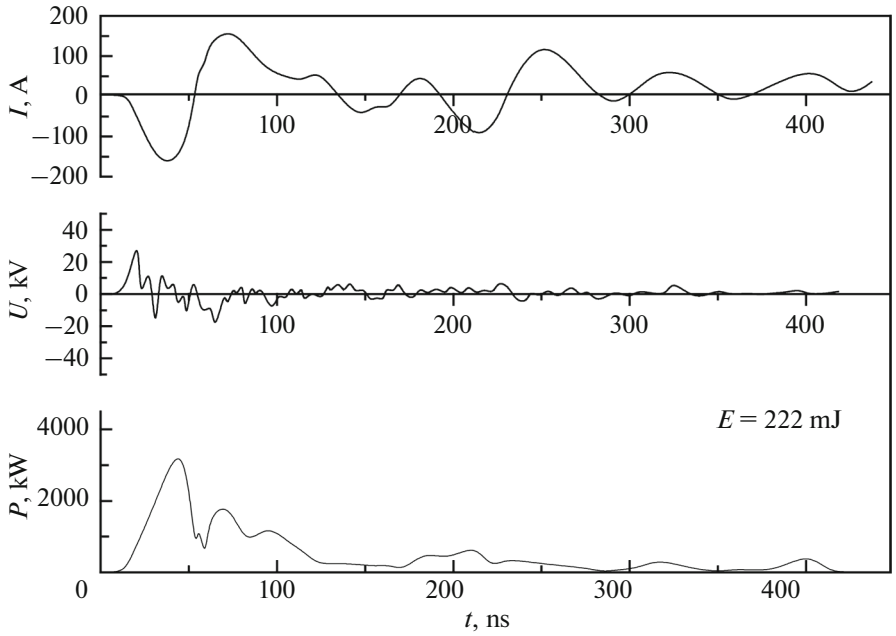

Fig. 2. Current, voltage, and pulsed power waveforms of the overstressed bipolar nanosecond discharge between electrodes of aluminum and chalcopyrite ($CuInSe_2$) at the air pressure of 101.3 kPa.

lations was approximately 70 ns. Short-term oscillations were better manifested on voltage waveforms. They were smoothed (integrated over time) on the current waveforms due to the large time constant of the Rogowski coil, which was used in the present experiments. The maximum voltage drop across the discharge gap was 8–10 kV taking into account the positive and negative parts of the voltage amplitude. The maximum amplitude of the current pulse reached 250–300 A.

The diffuse discharge most likely persists only in the first 80–120 ns from the time of the breakdown, and it passes into a contracted state after that; the same as during the ignition of an overstressed nanosecond discharge in air using negative-polarity pulses with a duration of 10 ns [9–11]. It is possible to obtain documentary confirmation of this assumption only when using high-speed photography of the discharge, when its appearance is recorded at different points in time with the nanosecond accuracy, but we only had the

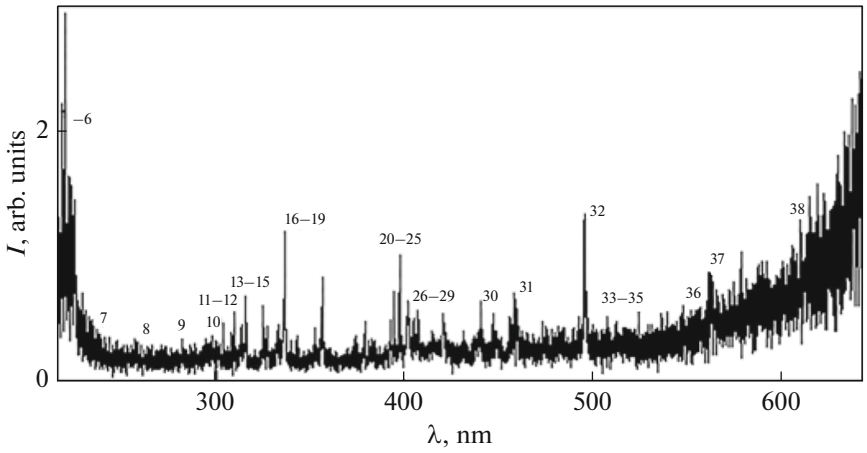

Fig. 3. Emission spectrum of the plasma of the overstressed nanosecond discharge between aluminum and chalcopyrite electrodes at the air pressure of 13.3 kPa.

opportunity to photograph the discharge with an exposure of ≈1 s.

Increasing the air pressure to 101.3 kPa led to an increase in the plasma resistance and improved its matching with the output resistance of the high-voltage modulator. As a result, the duration of the main maximum of the voltage pulse, which was recorded as a sequence of individual short beams, was reduced to 80 ns, and their amplitude increased to 12 kV. In this case, the duration of the current half-wave was reduced to 60–80 ns, and its maximum amplitude reached 300 A.

The highest discharge pulse power was recorded in the first 110–130 ns from the time of its ignition and it was 1.8 MW. An increase in air pressure from 13.3 to 101 kPa led to an increase in the maximum pulse power up to 3.0 MW, and the energy of an individual electrical pulse increased from 165 to 222 mJ (Figs. 1, 2).

OPTICAL CHARACTERISTICS

Control experiments on studying the spectral characteristics of plasma were carried out for overstressed discharge in air between two aluminum electrodes and between two ternary chalcopyrite electrodes [4, 20, 21]. Reference books [22–24] were used to identify spectral lines and emission bands.

The plasma emission spectra and the results of their interpretation for the discharge between aluminum and chalcopyrite electrodes at air pressures of 13.3 and 101.3 kPa, as well as the control spectrum for the discharge emission in argon, are shown in Figs. 3 and 4 and in Tables 1 and 2.

In the emission spectra of discharge in mixtures of air with an admixture of aluminum vapor [4] and in the spectra of plasma based on mixtures of nitrogen with oxygen, we recorded broad emission bands with maxima in the spectral intervals of 410–420 and 300–390 nm (Fig. 5). The highest emission intensity of these bands was obtained at a pressure of oxygen-containing gas mixtures of 100–200 kPa. For the discharge in argon-based mixtures, these bands were absent in the emission spectra of plasma. In [25], the results of studying the cathodoluminescence spectra of nanostructured aluminum oxide ceramics are presented. This cathodoluminescence spectrum was almost identical to the spectrum that was obtained in our experiments on studying overstressed nanosecond discharge emission at an air pressure in the range of 101–202 kPa or on mixtures of nitrogen with oxygen (p = 101.3 kPa; Fig. 5). In these spectra, the main emission band was with a maximum at λ = 410–420 nm (quantum energy of 3.0 eV), which was adjacent to a broader short-wavelength band with quanta energy maxima at E = 3.4, 3.8 and 4.3 eV. The ultraviolet photo- and cathodoluminescence bands of nanostructured aluminum oxide ceramics are associated with the emission of F^+ centers formed by oxygen vacancies [26].

At air pressures of 13.3 and 103.3 kPa, spectral lines of atoms and ions of the products of the electrode material and the decay of air molecules in plasma were observed against the background of broadband emission of aluminum oxide nanostructures and continuous radiation, which may be due to thermal and recombination radiation of the plasma. As follows from [27], copper and indium atoms are the least bound in the chalcopyrite molecule, so the line part of the emission spectrum is due mainly to individual spectral lines of atoms and singly charged ions of copper and indium, the same as for the gas-discharge plasma based on atmospheric pressure air [20]. The emission spectrum of the gas component was more pronounced at atmospheric air pressure and consisted mainly of intense bands of the second positive system of the nitrogen molecule in the spectral range of 280–390 nm, which is typical for the diffuse stage of the

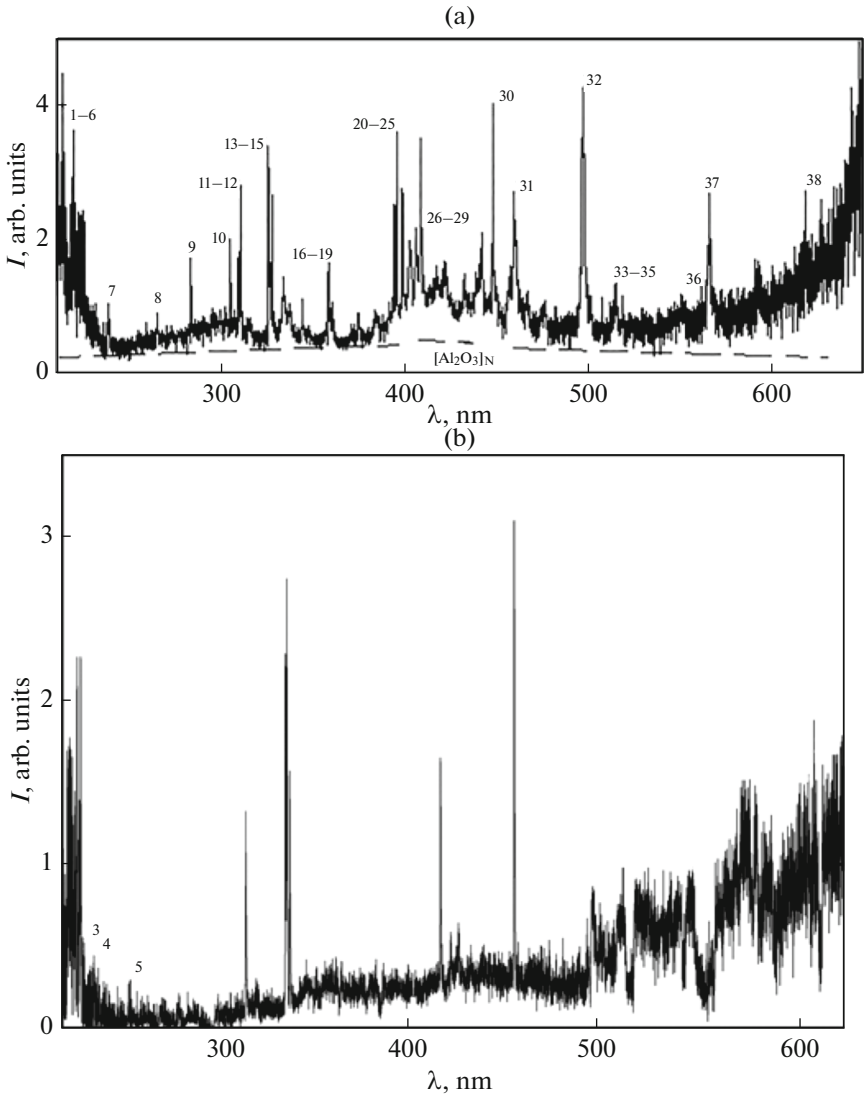

Fig. 4. Emission spectra of the overstressed nanosecond discharge between aluminum and chalcopyrite electrodes at the air pressure of (a) 101.3 kPa and in (b) argon at $p(\mathrm{Ar}) = 101.3$ kPa.

overstressed nanosecond discharge [9] as well as of individual spectral lines N(1) and N(11), which were often observed in the emission spectra of a spark discharge in air [28].

Therefore, in the plasma emission spectra of vapor–gas mixtures based on aluminum, dissociation products of the chalcopyrite molecule, air, and dissociation products of its molecules, the plasma emission spectrum in the wavelength range of 200–240 nm consisted of a group of closely spaced spectral lines of the atom and singly charged ion of copper, and lines of the atom and singly charged ion of aluminum (spectral lines *1–7*; Tables 1, 2). The spectral lines of copper were similar to those observed in the emission spectra of the overstressed nanosecond discharge between copper or chalcopyrite electrodes in air at the atmospheric pressure at a distance between copper electrodes of $d = 1$, 2 mm [20].

Another group of intense spectral lines and bands is located in the spectral range of 250–390 nm (lines and bands *8–20*; Tables 1, 2). For this region of the spectrum, the most characteristic were the spectral lines of copper and aluminum atoms as well as bright bands of the second positive system of the nitrogen molecule. The presence of intense bands of the nitrogen molecule from the system $C^3\Pi_u^+ - B^3\Pi_g^+$ indicates that, in addition to runaway electrons, the main part of the low-energy part of the electron energy distribution function also contains electrons with energies in the range of 9–18 eV, which are responsible for the emission of a nitrogen molecule in the spectral range of 290–410 nm.

Table 1. Results of the identification of the most intense spectral lines of an atom, a singly charged aluminum ion, and molecular bands of the decay products of a chalcopyrite molecule in an overstressed nanosecond discharge at an air pressure of 13.3 kPa

No.	λ, nm	I_{exp}, arb. units	Object	E_{bottom}, eV	E_{top}, eV	$Term_{bottom}$	$Term_{top}$
1	214.89	1.39	Cu(I)	1.39	7.18	$4s^2\ ^2D$	$5f\ ^2f^0$
2	218.17	1.98	Cu(I)	0.00	5.68	$4s\ ^2S$	$4p'\ ^2P^0$
3	219.56	1.87	Cu(II)	8.78	14.43	$4p\ ^3D^0$	$4d\ ^3f$
4	219.95	1.74	Cu(I)	1.39	7.02	$4s^2\ ^2D$	$4p''\ ^2D^0$
5	221.45	1.64	Cu(I)	1.39	6.98	$4s^2\ ^2D$	$4p''\ ^2P^0$
6	225.80	1.27	Al(I)	0.00	5.49	$3p\ ^2P^0$	$7s\ ^2s$
7	239.07	0.35	Al(II)	13.07	18.26	$4p\ ^3P^0$	$10d\ ^3D$
8	261.83	0.29	Cu(I)	1.39	6.12	$4s^2\ ^2D$	$5p\ ^2P^0$
9	284.02	0.25	Al(I)	4.02	8.39	$3d\ ^2D$	$3d\ ^2D^0$
10	306.34	0.35	Cu(I)	1.64	5.68	$4s^2\ ^2D$	$4p'\ ^2P^0$
11	308.21	0.47	Al(I)	0.00	4.02	$3p\ ^2P^0$	$3d\ ^2D$
12	309.27	0.55	Al(I)	0.01	4.02	$3p\ ^2P^0$	$3d\ ^2D$
13	324.75	0.61	Cu(I)	0	3.82	$4s\ ^2S$	$4p\ ^2P^0$
14	327.39	0.44	Cu(I)	0	3.39	$4s\ ^2S$	$4p\ ^2P^0$
15	329.05	0.45	Cu(I)	5.07	8.84	$4p'\ ^4f^0$	$4d'\ ^4f$
16	337.13	1.05	N_2	Second positive system $C^3\Pi_u^+$-$B^3\Pi_g^+$ (0; 0)			
17	344.60	0.31	N_2	″	″	″	$C^3\Pi_u^+$-$B^3\Pi_g^+$ (4; 5)
18	357.69	0.82	N_2	″	″	″	$C^3\Pi_u^+$-$B^3\Pi_g^+$ (0; 1)
19	375.54	0.31	N_2	″	″	″	$C^3\Pi_u^+$-$B^3\Pi_g^+$ (1; 3)
20	394.40	0.72	Al(I)	0.00	3.14	$3p\ ^2P^0$	$4s\ ^2S$
21	396.15	1	Al(I)	0.01	3.14	$3p\ ^2P^0$	$4s\ ^2S$
22	402.26	0.61	Cu(I)	3.79	6.87	$4p\ ^2P^0$	$5d\ ^2D$
23	405.67	0.48	Al(II)	15.47	18.52	$3s4d\ ^1D$	$3s15p\ ^1P^0$
24	409.48	0.39	N_2	″	″	″	$C^3\Pi_u^+$-$B^3\Pi_g^+$ (4; 8)
25	410.17	0.30	In(I)	–	3.02	$5s^25p\ ^2P^0$	$5s^26s\ ^2S_{1/2}$
26	420.05	0.50	N_2	″	″	″	$C^3\Pi_u^+$-$B^3\Pi_g^+$ (2; 6)
27	423.65	0.33	N_2	″	″	″	$C^3\Pi_u^+$-$B^3\Pi_g^+$ (1; 2)
28	434.36	0.38	N_2	″	″	″	$C^3\Pi_u^+$-$B^3\Pi_g^+$ (0; 4)
29	441.67	0.57	N_2	″	″	″	$C^3\Pi_u^+$-$B^3\Pi_g^+$ (3; 8)
30	451.13	0.54	In(I)	0.27	3.02	$5s^25p\ ^2P^0$	$5s^26s\ ^2s_{1/2}$
31	459.97	0.71	N_2	″	″	″	$C^3\Pi_u^+$-$B^3\Pi_g^+$ (2; 4)
32	500.51	1.33	N(II)	25.50	27.97	$3s\ ^5P$	$3p\ ^5P^0$
33	510.55	0.42	Cu(I)	1.39	3.82	$4s^2\ ^2D$	$4p\ ^2P^0$
34	515.83	0.47	Cu(I)	5.69	8.09	$4p'\ ^2P^0$	$5s'\ ^2D$
35	521.82	0.40	Cu(I)	3.82	6.19	$4p\ ^2P^0$	$4d\ ^2D$
36	556.69	0.55	Se(II)				
37	566.66	0.82	N(II)	18.46	20.65	$2s^2\ 2p\ 3s\ ^3P^0$	$2s^2\ 2p\ 3p\ ^3D$
38	618.86	1.18	Cu(II)	14.99	16.99	$4p''\ ^1D^0$	$5d\ ^3f$

Table 2. Results of the identification of the most intense spectral lines of an atom and a singly charged aluminum ion and molecular bands of the decay products of a chalcopyrite molecule in an overstressed nanosecond discharge at an air pressure of 101.3 kPa

No.	λ, nm	I_{exp}, arb. units	Object	E_{bottom}, eV	E_{top}, eV	$Term_{bottom}$	$Term_{top}$
1	214.89	4.60	Cu(I)	1.39	7.18	$4s^2\ ^2D$	$5f\ ^2F^0$
2	218.17	3.00	Cu(I)	0.00	5.68	$4s\ ^2S$	$4p'\ ^2P^0$
3	219.56	2.05	Cu(II)	8.78	14.43	$4p\ ^3D^0$	$4d\ ^3F$
4	219.95	3.60	Cu(I)	1.39	7.02	$4s^2\ ^2D$	$4p''\ ^2D^0$
5	221.45	2.75	Cu(I)	1.39	6.98	$4s^2\ ^2D$	$4p''\ ^2P^0$
6	225.80	2.30	Al(I)	0.00	5.49	$3p\ ^2P^0$	$7s\ ^2S$
7	239.07	1.00	Al(II)	13.07	18.26	$4p\ ^3P^0$	$10d\ ^3D$
8	261.83	0.88	Cu(I)	1.39	6.12	$4s^2\ ^2D$	$5p\ ^2P^0$
9	284.02	1.75	Al(I)	4.02	8.39	$3d\ ^2D$	$3d\ ^2D^0$
10	306.34	2.00	Cu(I)	1.64	5.68	$4s^2\ ^2D$	$4p'\ ^2P^0$
11	308.21	1.84	Al(I)	0.00	4.02	$3p\ ^2P^0$	$3d\ ^2D$
12	309.27	2.79	Al(I)	0.01	4.02	$3p\ ^2P^0$	$3d\ ^2D$
13	324.75	3.37	Cu(I)	0	3.82	$4s\ ^2S$	$4p\ ^2P^0$
14	327.39	3.10	Cu(I)	0	3.39	$4s\ ^2S$	$4p\ ^2P^0$
15	329.05	2.67	Cu(I)	5.07	8.84	$4p'\ ^4F^0$	$4d'\ ^4F$
16	337.13	1.47	N_2	Second positive system $C^3\Pi_u^+$-$B^3\Pi_g^+$ (0; 0)			
17	344.60	1.10	N_2	"	"	"	$C^3\Pi_u^+$-$B^3\Pi_g^+$ (4; 5)
18	357.69	1.68	N_2	"	"	"	$C^3\Pi_u^+$-$B^3\Pi_g^+$ (0; 1)
19	375.54	0.88	N_2	"	"	"	$C^3\Pi_u^+$-$B^3\Pi_g^+$ (1; 3)
20	394.40	2.49	Al(I)	0.00	3.14	$3p\ ^2P^0$	$4s\ ^2S$
21	396.15	3.63	Al(I)	0.01	3.14	$3p\ ^2P^0$	$4s\ ^2S$
22	402.26	2.77	Cu(I)	3.79	6.87	$4p\ ^2P^0$	$5d\ ^2D$
23	405.67	2.00	Al(II)	15.47	18.52	$3s4d\ ^1D$	$3s15p\ ^1P^0$
24	409.48	0.45	N_2	"	"	"	$C^3\Pi_u^+$-$B^3\Pi_g^+$ (4; 8)
25	410.17	0.37	In(I)	–	3.02	$5s^25p\ ^2P^0$	$5s^26s\ ^2S_{1/2}$
26	420.05	1.63	N_2	"	"	"	$C^3\Pi_u^+$-$B^3\Pi_g^+$ (2; 6)
27	423.65	1.69	N_2	"	"	"	$C^3\Pi_u^+$-$B^3\Pi_g^+$ (1; 2)
28	434.36	1.52	N_2	"	"	"	$C^3\Pi_u^+$-$B^3\Pi_g^+$ (0; 4)
29	441.67	2.10	N_2	"	"	"	$C^3\Pi_u^+$-$B^3\Pi_g^+$ (3; 8)
30	451.13	4.06	In(I)	0.27	3.02	$5s^25p\ ^2P^0$	$5s^26s\ ^2S_{1/2}$
31	459.97	2.73	N_2	"	"	"	$C^3\Pi_u^+$-$B^3\Pi_g^+$ (2; 4)
32	500.51	0.53	N(II)	25.50	27.97	$3s\ ^5P$	$3p\ ^5P^0$
33	510.55	0.46	Cu(I)	1.39	3.82	$4s^2\ ^2D$	$4p\ ^2P^0$
34	515.83	0.51	Cu(I)	5.69	8.09	$4p'\ ^2P^0$	$5s'\ ^2D$
35	521.82	0.58	Cu(I)	3.82	6.19	$4p\ ^2P^0$	$4d\ ^2D$
36	556.69	0.93	Se(II)				
37	566.66	2.65	N(II)	18.46	20.65	$2s^2\ 2p\ 3s\ ^3P^0$	$2s^2\ 2p\ 3p\ ^3D$
38	618.86	2.78	Cu(II)	14.99	16.99	$4p''\ ^1D^0$	$5d\ ^3F$

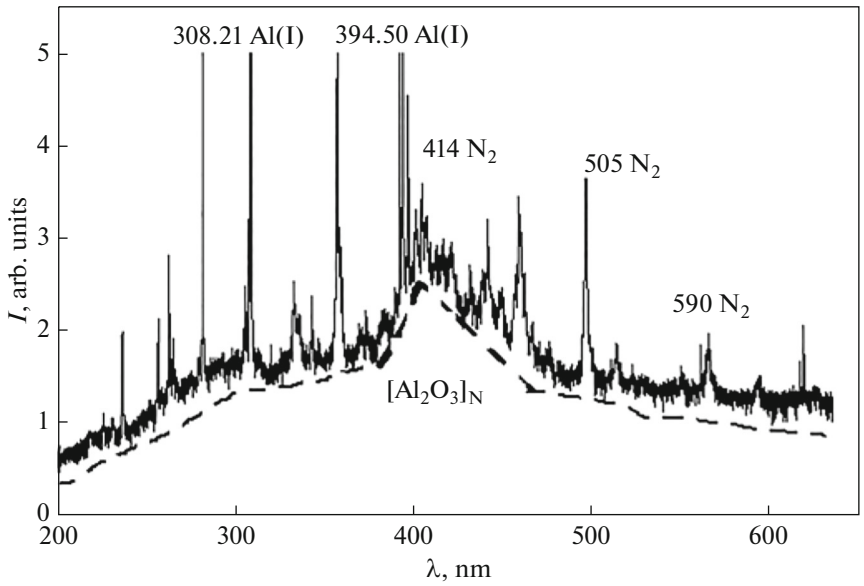

Fig. 5. Emission spectrum of the plasma of the overstressed nanosecond discharge between two aluminum electrodes in the mixture of nitrogen with oxygen (100-1; p = 101.3 kPa); dashed line, $[Al_2O_3]_N$, is notation of aluminum oxide nanoparticles.

Emission of indium atoms in the visible region of the spectrum was represented by spectral lines 410.17 and 451.13 nm In(I). An intense spectral line with a wavelength of 500.5 nm N(II) appeared in the emission spectrum of the plasma, which is often observed in the emission spectra of nanosecond discharges in air [2]. Characteristic spectral lines of the copper atom in the visible range of the spectrum of 510.55, 515.83, 521.04, and 556.69 nm Cu(I) were of low-intensity, unlike the plasma overstressed nanosecond discharge between copper electrodes in nitrogen or air, when the energy can be transferred from nitrogen molecules in the metastable states to copper atoms [10, 11]. In our case, radiation was sampled from the center of the discharge gap, and it was actually averaged over the entire discharge aperture, while radiation was sampled from the plasma jet region near the needle cathode in [10, 11].

In the red region of the spectrum, the spectral line of 618.86 nm Cu(II) was distinguished by the emission intensity, the intensity of which increased by a factor of 2.5 at increasing air pressure.

In the yellow-red part of the spectrum (Figs. 3, 4) a continuum was recorded, the intensity of which increased with increasing wavelength in the range of 550–665 nm and against which individual low-intensity spectral lines and molecular bands were observed that can be attributed to the emission of selenium molecules and their dissociation products in the discharge.

To diagnose the deposition of thin films of quaternary chalcopyrite in real time, the following intense spectral lines of copper and indium atoms in the wavelength range of 300–460 nm can be used: 307.38 and 329.05 nm Cu(I) and 410.17 and 451.13 nm In(I).

An increase in air pressure had a different effect on the intensity of different groups of spectral lines, products of the destruction of the electrode material. The maximum increase in intensity of 3.3 times was observed for the line λ = 214.89 nm of the most intense short-wavelength lines of the copper atom. For the intense copper ion line of 219.56, the increase in intensity was insignificant, by a factor of 1.1, although its intensity was the highest in this part of the spectrum. In the spectral region of 225–310 nm, the lines of the aluminum atom had the highest intensity, the most intense of which, 309.27 nm Al(I), increased in intensity. For the aluminum ion line from this region of the spectrum with λ = 239.07 nm Al(II), an increase in intensity was recorded by approximately three times. In the longer wavelength part of the spectrum of 310–410 nm, the most intense lines were 324.75, 327.39, and 329.05 nm Cu(I); 394.40 and 396.15 nm Al(I); and 405.67 nm Al(II). The intensity of all these lines increased by a factor of three to five with an increase in the air pressure. In the visible range of the spectrum, the most intense line of 451.13 nm In(I) increased in intensity by a factor of 7.5, and the intensity of the 405.67 nm Al(II) ion line increased by approximately five times.

The emission intensity of the ion spectral line with λ = 500.51 nm N(II) at the atmospheric air pressure decreased by a factor of 2.5, which may be due to a decrease in the electron temperature at air pressure p = 101.3 kPa, if the excitation of the nitrogen ion occurs from the ground state of the N_2 molecule, atom N(I), or ion N(II) (not a recombination mechanism for populating the upper energy level for a line with λ = 500.51 nm N(II)).

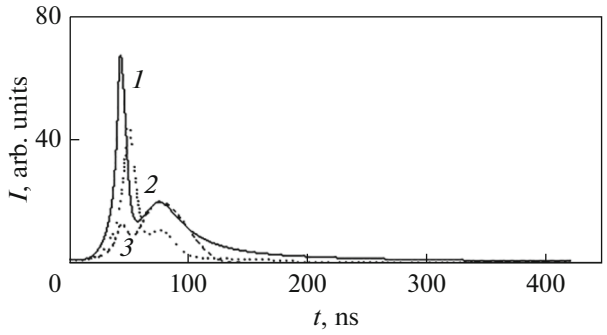

Fig. 6. Waveforms of the plasma emission on bands of the second positive system of the nitrogen molecule: (*1*) 337.13 nm N_2, (*2*) 357.69 nm N_2, (*3*) 375.54 nm N_2 for the overstressed nanosecond discharge in air (p = 101.3 kPa).

The electron density in the plasma of overstressed discharges of nanosecond duration and with an ecton sputtering mechanism of the electrode material [30] can reach 10^{16}–10^{17} cm^{-3} [31]. Therefore, the mechanism of the formation of excited metal ions in plasma can be determined by their stepwise excitation by electrons. Then, in the discharge afterglow, the electron-ion recombination processes begin to appear. For zinc ions, the corresponding effective cross section for the excitation by electrons from the ground state of the zinc ion reaches 10^{-16} cm^2 [32].

Based on the spiked structure of current pulses, the processes of stepped excitation and stepwise ionization through the corresponding metastable states, which are characteristic of high-current high-pressure discharges, seem important [33]. Therefore, a probable mechanism for the formation of doubly charged copper and aluminum ions in the ground energy state can be stepwise ionization of metastable atoms and ions of copper and aluminum by electrons.

An increase in air pressure can lead to an increase in the intensity of the spectral lines of copper and indium atoms and their singly charged ions due to an increase in the efficiency of the recombination mechanism at high buffer gas pressures [34] as well as in the processes of stepwise excitation and ionization of the corresponding atoms due to with an increase in the energy input into the plasma at atmospheric air pressure. The main feature of the introduction of copper and indium vapors into the plasma, which was studied, is not the reaction of dissociation of chalcopyrite molecules by electron impact, but the formation of excited atoms and singly charged ions of aluminum and argon in the processes of direct and stepwise electron excitation and ionization.

The increase in the intensity of the spectral line with λ = 405.67 nm Al(II) with increasing air pressure can be associated with an increase in the efficiency of recombination of doubly charged aluminum ions with electrons. The presence of such an effect in the plasma of spark discharges of the microsecond duration between aluminum electrodes can be indicated by the results of [35], where lines of doubly charged aluminum ions (λ = 371.3 nm Al(III) were observed in the plasma emission spectra. Aluminum in relation to air molecules and chalcopyrite is an easily excitable and easily ionized additive in this gas–vapor mixture. Therefore, with a significant probability, singly and doubly charged aluminum ions can be directly formed during microexplosions of natural inhomogeneities on the surface of an aluminum electrode [30].

Figure 6 shows emission waveforms of the plasma of the overstressed nano-second discharge in atmospheric pressure air at the transitions of the second positive band system of the nitrogen molecule. The total duration of the glow at these transitions of the nitrogen molecule, as in [5, 10, 11], where the characteristics of overstressed nanosecond of a monopolar discharge in the needle–plane system of electrodes were studied, was 80–120 ns at half maximum of the intensity amplitude. The glow in these bands of the nitrogen molecule occurs at the diffuse discharge stage before the arrival of reflected waves, which are formed due to mismatch between the plasma resistance and the output resistance of the high-voltage modulator. This discharge stage on the luminescence waveforms corresponds to the first maximum with a duration of 15–20 ns at half maximum of the intensity (Fig. 6).

TRANSMISSION SPECTRA OF SYNTHESIZED FILMS

In the wavelength range of λ = 200–400 nm, the absorption coefficient of thin films of ternary chalcopyrite $CuInSe_2$ is significant and lies within (4–6) × 10^5 cm^{-1} [36]. As the emission wavelength increased to 1000 nm, it decreased to 10^4 cm^{-1}, and it was approximately 10 cm^{-1} at λ = 1200 nm. That is, the coefficient of light absorption by the films of this compound is large but strongly depends on the wavelength of the incident radiation, which is reflected in its applications in photovoltaic devices. This also implies the importance of expanding the $CuInSe_2$ band gap and increasing the absorption coefficient in the near infrared region of the spectrum, which can be implemented by transforming the $CuInSe_2$ compound in the form of a massive electrode into thin films of quaternary chalcopyrite $CuAlInSe_2$ [17].

The characteristic transmission spectra of ultraviolet (UV) radiation by the thin films we synthesized (probably based on the $CuAlInSe_2$ compound) in the spectral region λ = 200–500 nm are shown in Fig. 7. The transmission spectra of the synthesized films were obtained by passing UV radiation from a deuterium lamp through them [37].

The transmission of thin films we synthesized in comparison with the transmission of the substrate decreased by approximately four times and it was minimal for the film that was synthesized from the plasma

at the atmospheric air pressure in the discharge chamber. The shapes of the transmission spectra for thin films synthesized at air pressures of 13.3 and 101.3 kPa were similar. The decrease in the transmission of a thin film that was synthesized at atmospheric air pressure, compared with the transmission of a film synthesized at $p = 13.3$ kPa, is due to an increase in the energy input into the atmospheric pressure discharge and, accordingly, an increase in the amount of the dispersed electrode material.

When replacing a gas-discharge deuterium lamp with a thermal one, the transmission spectra of the same films based on aluminum vapor and ternary chalcopyrite were studied in the spectral range $\lambda = 400–800$ nm. In this case, the main features of the transmission spectra of the thin films we synthesized at different air pressures also correlated with those results for the UV range of the spectrum shown in Fig. 7.

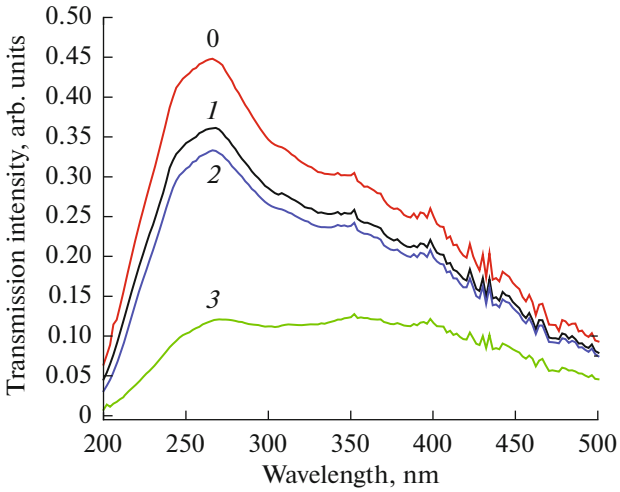

Fig. 7. Transmission spectra of the radiation of films synthesized from the plasma based on vapors of aluminum and ternary chalcopyrite at different air pressures in the discharge chamber at their probing with the UV radiation of the deuterium lamp: (0) no sample; (*1*) pure quartz substrate; (*2*) electrodes: one of $CuInSe_2$, another of aluminum at the air pressure of 13.3 kPa; (*3*) electrodes: one of $CuInSe_2$, another of aluminum at the air pressure of 101.3 kPa.

NUMERICAL SIMULATION OF PLASMA PARAMETERS

A standard program for solving the stationary kinetic Boltzmann equation in a two-term approximation for the electron energy distribution function (EEDF) was chosen for the numerical simulation of plasma parameters of air at pressures of 13.3 and 101.3 kPa and with impurities of aluminum and copper vapors at pressures of 100 and 10 000 Pa. Parameters of the plasma discharge in mixtures of air, argon with aluminum, and copper vapors were calculated numerically as full integrals from EEDF. The EEDFs were found by solving the Boltzmann kinetic equation in a two-term approximation. The EEDF calculations were carried out using the program [38], where the database of effective cross sections also includes the effective cross sections for the interaction of electrons with copper atoms and air components. The effective cross sections for the interaction of electrons with aluminum atoms were taken from [39]. For air, four components were selected: argon, nitrogen, carbon dioxide, and oxygen; the effective cross sections of the processes for these components were taken from the program database [38]. Based on the calculated EEDF, the main plasma parameters were determined depending on the reduced electric field E/N (that is, the ratio of the electric field strength (E) to the total concentration of air and impurities of aluminum and copper vapors (N)). The range of the variation of the parameter for a mixture of air with admixtures of aluminum and copper vapors was in the range of $E/N = 1–2500$ Td ($1 \times 10^{-17} – 2.5 \times 10^{-14}$ V cm^2) and also included the parameter E/N, which was implemented in the experiment. In the integral of collisions of electrons with molecules and atoms, the following processes were taken into account: elastic scattering of electrons by argon, nitrogen, carbon dioxide, oxygen, aluminum, and copper atoms; excitation of energy levels of argon atoms (threshold energy of 11.50 eV); ionization of argon atoms (energy threshold of 15.80 eV); excitation of the rotational level of nitrogen molecules (threshold energy of 0.020 eV), vibrational (threshold energies: 0.290, 0.291, 0.590, 0.880, 1.170, 1.470, 1.760, 2.060, 2.350 eV), and electron (threshold energies: 6.170, 7.000, 7.350, 7.360, 7.800, 8.160, 8.400, 8.550, 8.890, 11.03, 11.87, 12.25, 13.00 eV); ionization (threshold energy of 15.60 eV); excitation of energy levels of oxygen molecules: vibrational (threshold energies of: 0.190, 0.380, 0.570, 0.750 eV), electron (threshold energies of: 0.977, 1.627, 4.500, 6.000, 8.400, 9.970 eV); dissociative electron attachment (threshold energy of 4.40 eV); ionization (threshold energy of 12.06 eV); excitation of energy levels of carbon dioxide molecules: vibrational (threshold energy of: 0.083, 0.167, 0.252, 0.291, 0.339, 0.422, 0.505, 2.5 eV), electron (threshold energies of: 7.0, 10.5 eV); dissociative electron attachment (threshold energy of 3.85 eV); ionization (threshold energy of 13.30 eV); excitation of energy levels of aluminum atoms (threshold energies of: 3.1707, 2.9032, 4.1463, 4.2339, 4.1296, 5.1220 eV); ionization of aluminum atoms (energy threshold of 6.0000 eV); excitation of energy levels of copper atoms (threshold energies of: 1.500, 3.800, 5.100 eV); ionization of copper atoms (threshold energy of 7.724 eV).

Figure 8 shows the dependences of the average energy of electrons in the plasma discharge in air mixtures for pressures of 101 and 13.3 kPa with admixtures of aluminum and copper vapors at pressures of 100 Pa and 10 kPa on the reduced electric field strength. The average discharge electron energy for all mixtures increases linearly from: 0.15 to 16.47 eV (Fig. 8 (*1*)) for

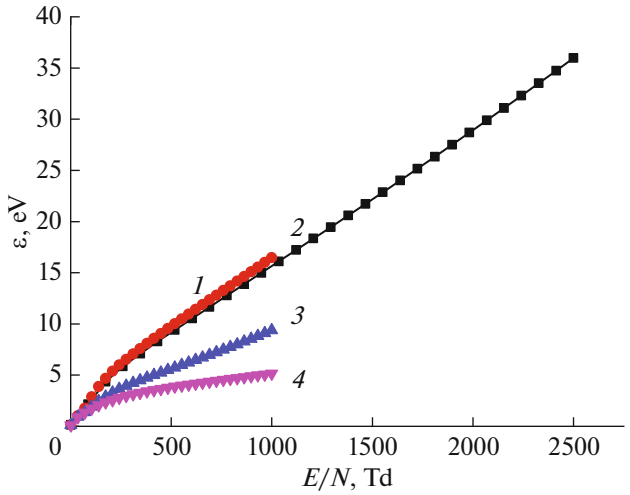

Fig. 8. Dependence of the average energy of electrons in the plasma of gas-vapor mixtures on the reduced electric field strength: (*1*) air–Al–Cu = 101300–100–100 at the total pressure of 101 500 Pa; (*2*) air–Al–Cu = 13300–100–100 Pa at the total pressure of 13500 Pa; (*3*) air–Al–Cu = 101300–10000–10000 at the total pressure of 121300 Pa; (*4*)air–Al–Cu = 13300–10000–10000 at the total pressure of 33300 Pa.

air–Al–Cu = 101 300–100–100 Pa, from 0.14 to 35.98 eV (Fig. 8 (*2*)) for air–Al–Cu = 13300–100–100 Pa, from 0.11 to 9.39 eV (Fig. 8 (*3*)) for air–Al–Cu = 101300–10000–10000 Pa, from 0.08 to 5.24 eV (Fig. 8 (*4*)) for air–Al–Cu = 13300–10000–10000 Pa with an increase in the reduced electric field strength from 1 to 1000 Td and from 1 to 2500 Td for a mixture of air–Al–Cu = 13300–100–100 Pa. At the same time, a pattern was observed of an increase in the rate of its change in the range of the reduced electric field strength of 1–150 Td for all mixtures. Table 3 shows the results of calculating the transport characteristics of electrons: average energies (ε), temperature (*T*, K), drift velocity

(V_{dr}), and electron density for four mixtures of air and aluminum and copper vapors. The average energy of discharge electrons for the air–aluminum–copper vapor–gas mixture = 101.3 kPa–100 Pa at a time of 30 ns from the beginning of the pulse ($E = 15 \times 10^6$ V/m, $E/N = 612$ Td) reached 11.42 eV, and the average energy of discharge electrons was 5.38 eV at a time of 220 ns from the beginning of the pulse ($E = 5 \times 10^6$ V/m, $E/N = 204$ Td). As the partial pressures of metals increase, the average energy decreases to 5.739 and 2.908 eV, respectively. The same pattern is observed for the electron temperature; it decreases with increasing partial pressures of aluminum and copper vapors. With a decrease in the partial pressure of air to 13.3 kPa, the average electron energies for a mixture with a partial pressure of metal vapors of 100 Pa are higher than for a mixture with a partial pressure of air of 101.3 kPa; they reach 35.98 and 14.99 eV, respectively. With an increase in the partial pressures of alu-

Table 3. Transport characteristics of electrons in a discharge in a mixture of air with aluminum and copper vapors at a ratio of components 101.3 kPa:100 Pa:100 Pa; 101.3 kPa:10000 Pa: 10000 Pa; 13.3 kPa: 10000 Pa: 10000 Pa; 13.3 kPa: 100 Pa: 100 Pa for a time of 30 ns and 220 ns from the start of the discharge ignition

τ, ns	*E/N*, Td	Mixture: Al–Cu–air = 100–100–101300 Pa			
		ε, eV	*T*, K	V_{dr}, m/s	N_e, m^{-3}
30	612	11.42	132472	4.6×10^5	1.0×10^{20}
220	204	5.38	62408	2.1×10^5	7.7×10^{20}
τ, ns	*E/N*, Td	Mixture: Al–Cu–air = 10000–10000–101300 Pa			
		ε, eV	*T*, K	V_{dr}, m/s	N_e, m^{-3}
30	512	5.739	66572	3.1×10^5	1.6×10^{20}
220	171	2.908	33733	1.6×10^5	1.0×10^{20}
τ, ns	*E/N*, Td	Mixture: Al–Cu–air = 100–100–13300 Pa			
		ε, eV	*T*, K	V_{dr}, m/s	N_e, m^{-3}
30	2500	35.98	417368	1.1×10^6	3.75×10^{19}
220	938	14.99	173884	5.9×10^5	3.81×10^{19}
τ, ns	*E/N*, Td	Mixture: Al–Cu–air = 10000–10000–13300 Pa			
		ε, eV	*T*, K	V_{dr}, m/s	N_e, m^{-3}
30	1000	5.24	60784	3.4×10^5	1.21×10^{20}
220	375	3.28	38048	2.5×10^5	9.00×10^{19}

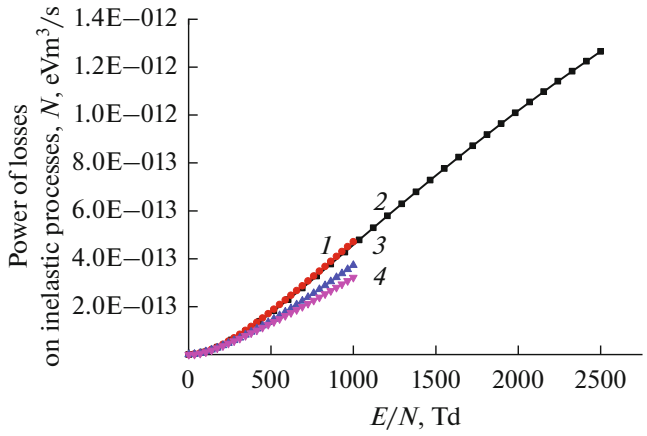

Fig. 9. Dependence of the specific power of discharge losses on inelastic processes of collisions of electrons with atoms of argon, aluminum, and copper on the reduced electric field strength in the plasma of vapor–gas mixtures: (*1*) air–Al–Cu = 101 300–100–100 Pa at the total pressure of 101 500 Pa; (*2*) air–Al–Cu = 13 300–100–100 Pa at the total pressure of 13 500 Pa; (*3*) air–Al–Cu = 101 300–10 000–10 000 at the total pressure of 121 300 Pa; (*4*) air–Al–Cu = 13 300–10 000–10 000 at the total pressure of 33 300 Pa.

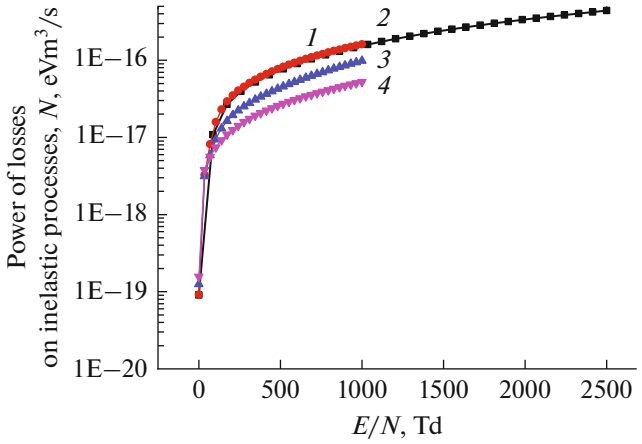

Fig. 10. Dependence of the specific power of discharge losses on elastic processes of collisions of electrons with atoms of argon, aluminum, and copper on the reduced electric field strength in the plasma of vapor–gas mixtures: (*1*) air–Al–Cu = 101 300–100–100 Pa at the total pressure of 101 500 Pa; (*2*) air–Al–Cu = 13 300–100–100 Pa at the total pressure of 13 500 Pa; (*3*) air–Al–Cu = 101 300–10 000–10 000 at the total pressure of 121 300 Pa; (*4*) air–Al–Cu = 13 300–10 000–10 000 at the total pressure of 33 300 Pa.

minum and copper to 10 kPa at a partial air pressure of 13.3 kPa, the average electron energies decrease and reach 5.24 and 3.28 eV, respectively. The electron temperatures for a smaller value of the partial air pressure also decrease with an increase in the partial pressures of aluminum and copper. The electron drift velocities have a similar regularity as the average electron energies with a change in the partial pressures of the gas-vapor mixture components. The maximum electron drift velocity is 1.1×10^6 m/s for the air–Al–Cu mixture = 13 300–100–100 Pa for the reduced electric field of 2500 Td. The maximum electron density for

Table 4. Specific power losses of the discharge to elastic and inelastic processes for mixtures: (*1*) air–Al–Cu = 101 300–100–100 at the total pressure of 101 500 Pa; (*2*) air–Al–Cu = 13 300–100–100 Pa at the total pressure of 13 500 Pa; (*3*) air–Al–Cu = 101 300–10 000–10 000 at the total pressure of 121 300 Pa; (*4*) air–Al–Cu = 13 300–10 000–10 000 at the total pressure of 33 300 Pa

Mixture: Al–Cu–air = 100–100–101 300 Pa		
E/*N*, Td	Elastic, power/*N* (eV m^3/s)	Inelastic, power/*N* (eV m^3/s)
612	0.9841E-16	0.2473E-12
204	0.3501E-16	0.4278E-13
Mixture: Al–Cu–air = 100–100–13 300 Pa		
E/*N*, Td	Elastic, power/*N* (eV m^3/s)	Inelastic, power /N (eV m^3/s)
2500	0.4404E-15	0.1266E-11
938	0.1458E-15	0.4279E-12
Mixture: Al–Cu–air = 10 000–10 000–101 300 Pa		
E/*N*, Td	Elastic, power/*N* (eV m^3/s)	Inelastic, power/*N* (eV m^3/s)
512	0.4570E-16	0.1482E-12
171	0.1631E-16	0.2822E-13
Mixture: Al–Cu–air = 10 000–10 000–13 300 Pa		
E/*N*, Td	Elastic, power/*N* (eV m^3/s)	Inelastic, power/*N* (eV m^3/s)
1000	0.5253E-16	0.3217E-12
375	0.2076E-16	0.8997E-13

Table 5. Rate constants of excitation of the spectral lines of aluminum and copper atoms for the reduced electric field strengths in the plasma on gas-vapor mixtures of argon with aluminum at the time of 30 and 220 ns from the beginning of discharge ignition. E_{thres} is the excitation threshold energy of spectral lines of aluminum and copper atoms

E/N, Td	Mixture: air–Al–Cu = 1330–100–100 Pa					
2500	Al	E_{thres}, eV	4.13	4.23	2.90	3.17
		k, m^3/s	0.1593E-14	0.1823E-14	0.2629E-14	0.4626E-14
	Cu	E_{thres}, eV	1.5	1.5	3.8	5.1
		k, m^3/s	0.2136E-13	0.1696E-13	0.9967E-12	0.2967E-15
938	Al	E_{thres}, eV	4.13	4.23	2.90	3.17
		k, m^3/s	0.1569E-14	0.1925E-14	0.2248E-14	0.4082E-14
	Cu	E_{thres}, eV	1.5	1.5	3.8	5.1
		k, m^3/s	0.2850E-13	0.2253E-13	0.8285E-12	0.2185E-15
E/N, Td	Mixture: air–Al–Cu = 101300–100–100 Pa					
612	Al	E_{thres}, eV	4.13	4.23	2.90	3.17
		k, m^3/s	0.1476E-14	0.1881E-14	0.2031E-14	0.3766E-14
	Cu	E_{thres}, eV	1.5	1.5	3.8	5.1
		k, m^3/s	0.2835E-13	0.2215E-13	0.6958E-1	0.1821E-15
204	Al	E_{thres}, eV	4.13	4.23	2.90	3.17
		k, m^3/s	0.8646E-15	0.1280E-14	0.1272E-14	0.2548E-14
	Cu	E_{thres}, eV	1.5 eV	1.5 eV	3.8 eV	5.1 eV
		k, m^3/s	0.1756E-13	0.1319E-13	0.2767E-12	0.7435E-16
E/N, Td	Mixture: air–Al–Cu = 101300–10000–10000 Pa					
512	Al	E_{thres}, eV	4.13	4.23	2.90	3.17
		k, m^3/s	0.9356E-15	0.1423E-14	0.1438E-14	0.2896E-14
	Cu	E_{thres}, eV	1.5	1.5	3.8	5.1
		k, m^3/s	0.1895E-13	0.1420E-13	0.2892E-12	0.7836E-16
171	Al	E_{thres}, eV	4.13	4.23	2.90	3.17
		k, m^3/s	0.2233E-15	0.4172E-15	0.6621E-15	0.1434E-14
	Cu	E_{thres}, eV	1.5	1.5	3.8	5.1
		k, m^3/s	0.5410E-14	0.3857E-14	0.5080E-13	0.1397E-16

air–Al–Cu mixtures is 101 300–100–100 Pa. Its value is 7.7×10^{20} m^{-3}.

Figures 9 and 10 show the dependence of the specific power of discharge losses on inelastic and elastic processes of collisions of electrons with mixture components in a gas-discharge plasma on the reduced electric field strength. There is a regularity of the power increase with the increase in the reduced electric field strength for inelastic and elastic processes. For inelastic processes, discharge losses in the range of 1–400 Td are approximately the same, and they vary within $(2–5) \times 10^{-13}$ eV m^3/s in the range of 400–1000 Td. For elastic processes, discharge losses differ starting from 1 Td, and the difference between their values increases with the increase in the reduced electric field strength. In addition, there is a regularity of power losses for inelastic and elastic processes of electron collisions with mixture components, namely, they are the same for mixtures with lower partial pressures of aluminum and copper vapors. A similar regularity may be associated with high electron energies in such mixtures (Table 3) and close constants of inelastic and elastic processes in mixtures with lower partial pressures of aluminum and copper vapors (Table 4).

Table 5 shows the rate constants of excitation of individual spectral lines of aluminum and copper atoms by discharge electrons in the studied vapor-gas mixtures for the reduced electric field strengths, which were at the time of 30 and 220 ns from the beginning of the discharge ignition, having the excitation thresh-

old energy of the spectral lines (E_{thres}) of 4.13, 4.23, 2.90, 3.17 eV for aluminum atoms and 1.5, 1.5, 3.8, 5.1 eV for copper atoms. They vary in the range of 0.1397E-16–0.9967E-12 m^3/s for the characteristic values of the reduced electric field strength. At the same time, their value for copper atoms is higher than the values for aluminum atoms in all the studied mixtures. The increased values of the excitation rate constants for the spectral lines of both aluminum atoms and copper atoms at the time from the beginning of discharge ignition (30 ns) compared to the time of 220 ns are also characteristic. This regularity is explained by different reduced electric field strength values for the time 30 and 220 ns (Figs. 1, 2) and, respectively, different average electron energies (Table 3), which leads to different absolute values of the effective cross sections of inelastic collisions of electrons with copper and aluminum atoms. The effective cross sections of inelastic electron collisions for copper atoms are larger than those for aluminum atoms [38, 30], and therefore, the excitation rate constants of lines for copper atoms are large as well.

CONCLUSIONS

It is shown that an overstressed nanosecond discharge is ignited between an aluminum electrode and an electrode from the $CuInSe_2$ compound at a distance between electrodes of 1 mm and an air pressure of 13.3 and 101.3 kPa. The discharge has a pulsed electric power of up to 3.0 MW and an energy input into the plasma per discharge pulse of up to 0.22 J.

The study of the spectral characteristics of the plasma based on vapor–gas air–Al–$CuInSe_2$ mixtures showed that the spectral lines of the atom and singly charged ion of copper in the range of λ = 200–225 nm and the spectral lines of atoms and singly charged ions of aluminum in the wavelength range of λ = 225–310 nm, as well as the lines of the aluminum, indium and copper atoms in the region of the spectrum of λ = 310–525 nm, are the most intense. The 618.86 nm Cu(II) line stood out from the ion lines in the spectrum. All spectral lines of metal atoms and ions, which were a part of the electrode material, were observed against the background of a wide emission band of aluminum oxide nanostructures. An increase in the air pressure from 13.3 to 101.3 kPa led mainly to the increase in the intensity of the spectral lines of metals and bands of the nitrogen molecule.

For the real-time diagnostics of deposition of quaternary chalcopyrite ($CuIn_{1-x}Al_xSe_2$) films, the following separately placed intense spectral lines can be used: 307.38, 329.05 nm Cu(I); 410.17, 451.13 nm In(I); 308.21, 309.27, 394.40, 396.15 nm Al(I). The presence of the main spectral lines of aluminum, copper, and indium in the emission spectra of the plasma makes it possible to assume the possibility of the deposition of a film of quaternary chalcopyrite outside the plasma medium, as was implemented for films of ternary chalcopyrite.

The study of the transmission spectra of probing radiation in the wavelength range of λ = 200–800 nm by films based on aluminum and ternary chalcopyrite vapors, which were synthesized by the in-air pulsed gas-discharge method, showed that the minimum is the transmission for films synthesized at the atmospheric air pressure; it is probable that the films synthesized from the plasma based on aluminum vapors and the decomposition products of the ternary chalcopyrite $CuInSe_2$ molecules belong to the quaternary chalcopyrite $CuAlInSe_2$.

The study of the transport characteristics of electrons and the power losses of the discharge to elastic and inelastic processes of collisions of electrons with the components of gas–vapor mixtures of air with copper and aluminum atoms established that the average electron energies and temperatures in the discharge on mixtures with lower partial pressures of air, aluminum, and copper vapors have greater values than those in the discharge on mixtures with high partial pressures of their components. In addition, the increased electron average energies and temperatures are observed, which were at the time of 30 ns from the beginning of the discharge ignition compared to the time of 220 ns for all mixtures studied. The maximum values of the electron's average energy and temperature were 35.98 eV and 417 368 K, respectively, for the discharge in the air–Al–Cu mixture = 13 300–100–100 Pa. The discharge power losses on elastic and inelastic processes of collisions of electrons with the components of gas-vapor mixtures have a similar regularity. They are large in terms of the values for the reduced electric field strengths, which were at the beginning of the discharge ignition, and have large values for the inelastic processes of electron collisions with the components of vapor-gas mixtures. The maximum value (0.1266×10^{-11} eV m^3/s) is also observed for air–Al–Cu mixtures = 13 300–100–100 Pa. The increased excitation rate constants for the spectral lines of aluminum atoms and copper atoms at the time from the beginning of discharge ignition (30 ns) compared to the time of 220 ns for all vapor-gas mixtures are also characteristic. Their values are within 0.1397E-16–0.9967E-12 m^3/s. Due to the fact that in the air–Al–Cu mixture = 13 300–100–100 Pa, the large excitation rate constants of the spectral lines of aluminum and copper atoms are observed, which ensures their high intensity in the discharge, it is recommended to use such a mixture for diagnostics and deposition of the corresponding films.

CONFLICT OF INTEREST

The authors declare that they have no conflicts of interest.

REFERENCES

1. Babich, L.P., Loiko, T.V., and Tsukerman, V.A., High-voltage nanosecond discharge in a dense gas at a high overvoltage with runaway electrons, *Sov. Phys.-Usp.,* 1990, vol. 33, no. 7, p. 521. https://doi.org/10.1070/PU1990v033n07ABEH002606
2. Shuaibov, A.K., Minya, A.Y., Gomoki, Z.T., Hrytsak, R.V., et al., Spectroscopic study of the decomposition of a chalcopirite molecule in a overstressed nanosecond discharge on a mixture of nitrogen with $CuInSe_2$ vapor compound, *J. Phys. Chem. Res.,* 2019, vol. 1, no. 2, p. 1.
3. Shuaibov, A.K., Minya, A.Y., Gomoki, Z.T., Malinina, A.A., et al., Plasma reactor generating synchronous flows of bactericidal UV radiation and nanostructures of zinc, copper, iron oxides and chalcopyrite, *HSOA J. Biotech Res. Biochem.,* 2020, vol. 3, no. 1, p. 1.
4. Shuaibov, A.K., Minya, A., Malinina, A., Malinin, A., et al., Synthesis of aluminum oxide nanoparticles in overstressed nanosecond discharge plasma with the ectonic sputtering mechanism of aluminum electrodes, *Highlights BioSci.,* 2020, vol. 3, p. 20211. https://doi.org/10.36462/H.BioSci.20211
5. Beloplotov, D.V., Tarasenko, V.F., and Lomaev, M.I., Luminescence of atoms and ions of aluminum in pulse-periodic nanosecond discharge initiated by runaway electrons in nitrogen, *Opt. Atmos. Okeana,* 2016, vol. 29, no. 2, p. 96. https://doi.org/10.15372/AOO20160202
6. Dadras, S., Tovkamany, M.J., and Subbaghzden, J., Characterization and comparison of iron and aluminium laser ablation with time-integrated emission spectroscopy of induced plasma, *J. Phys. D Appl. Phys.,* 2008, vol. 41, p. 225202.
7. Beloplotov, D.V., Trigub, M.V., Tarasenko, V.F., Evtushenko, G.S., et al., Laser monitor visualization of gas-dynamic processes under pulse-periodic discharges initiated by runaway electrons in atmospheric pressure air, *Atmos. Ocean. Opt.,* 2016, vol. 29, p. 371. https://doi.org/10.1134/S1024856016040047
8. Tren'kin, A.A., Almazova, K.I., Belonogov, A.N., Borovkov, V.V., et al., Dynamics of the initial stage of the spark and diffuse discharges in air in a point–plane gap at different parameters of the tip electrode, *Tech. Phys.,* 2019, vol. 64, no. 4, p. 470. https://doi.org/10.1134/S1063784219040261
9. Beloplotov, D.V., Lomaev, M.I., Sorokin, D.A., and Tarasenko, V.F., Streamers at the subnanosecond breakdown of argon and nitrogen in nonuniform electric field at both polarities, *Tech. Phys.,* 2018, vol. 63, no. 6, p. 793. https://doi.org/10.1134/S1063784218060063
10. Beloplotov, D.V., Lomaev, M.I., Sorokin, D.A., and Tarasenko, V.F., Blue and green jets in laboratory discharges initiated by runaway electrons, *J. Phys. Conf. Ser.,* 2015, vol. 652, p. 012012. https://doi.org/10.1088/1742-6596/652/1/012012
11. Lomaev, M., Beloplotov, D., Sorokin, D., and Tarasenko, V., The radiative properties of plasma of pulse-periodic discharge initiated with runaway electrons, *32nd Int. Conf. on Phenomena in Ionized Gases,* Iasi, Romania, July 26–31, 2015.
12. Kostyrya, I.D., Tarasenko, V.F., and Rybka, D.V., Peculiarities of registration of runaway electrons during the breakdown of air at atmospheric pressure by voltage pulses with a leading edge of 0.5 μs, *Izv. Vyssh. Uchebn. Zaved. Fiz.,* 2014, vol. 57, no. 12/2, p. 220.
13. Korenyugin, D.G., Martsinovsky, A.M., and Orlov, K.E., Field electron emission from cathode as a possible factor in the transition from a streamer to spark discharge channel, *Tech. Phys. Lett.,* 2009, vol. 35, no. 10, p. 944.
14. Laux, C.O., Spence, T.G., Kruger, C.H., and Zave, R.N., Optical diagnostics of atmospheric pressure air plasmas, *Plasma Sources Sci. Technol.,* 2003, vol. 12, p. 125. https://doi.org/10.1088/0963-0252/12/2/301
15. Kudryavyi, V.G., Obtaining nanodispersed oxides and functional materials in plasma of a pulsed high-voltage discharge, *Vestn. Dal'nevost. Otd. Russ. Akad. Nauk,* 2009, no. 2, p. 53.
16. Vincent A. Vons, Louis C.P.M. de Smet, David Munao, et al., Silicon nanoparticles produced by spark discharge, *J. Nanopart. Res.,* 2011, vol. 13, p. 4867. https://doi.org/10.1007/s11051-011-0466-0
17. Lopez-Garcia, J., Placidi, M., Fontane, X., Izguierdo-Roca, V., et al., $CuIn_{1-x}Al_xSe_2$ thin film solar cells with depth gradient compositions prepared by selenization of evaporated metallic evaporated precursors, *Sol. Energy Mater. Sol. Cells*, 2015, vol. 132, p. 245.
18. Shuaibov, A.K., Minya, A.I., Gritsak, R.V., et al., Characteristics of the nanosecond overvoltage discharge between $CuInSe_2$ chalcopyrite electrodes in oxygen-free gas media, *Ukr. J. Phys.*, 2020, vol. 65, no. 5, p. 400. https://doi.org/10.15407/ujpe65.5.400
19. Tarasenko, V.F., *Runaway Electrons Preionized Diffuse Discharge,* New York: Nova Science, 2014.
20. Shuaibov, O.K., Malinina, A.O., and Malinin, O.M., *Novi hazorozryadni metody oderzhannya selektyvnoho ul'trafioletovoho i vydymoho vyprominyuvannya ta syntezu nanostruktur oksydiv perekhidnykh metaliv. Monohrafiya* (New Gas-Discharge Methods for Obtaining Selective Ultraviolet and Visible Radiation and Synthesis of Nanostructures of Transition Metal Oxides. Monograph), Uzhhorod: Vyd. Uzhhorod. Nats. Univ. Hoverla, 2019
21. Shuaibov, A.K., Minya, A.Y., Hrytsak, R.V., Malinina, A.A., et al., Characteristics of an overstressed discharge of nanosecond duration between electrodes of chalcopyrite in high pressure nitrogen, *Adv. Nanosci. Nanotechnol.,* 2020, vol. 4, no. 1, p. 1. https://doi.org/10.33140/ANN.04.01.01
22. Striganov, A.R. and Sventitskii, N.S., *Tablitsy spektral'nykh linii neitral'nykh i ionizirovannykh atomov* (Tables of Spectral Lines of Neutral and Ionized Atoms), Moscow: Atomizdat, 1966.
23. NIST Atomic Spectra Database Lines Form. https://physics.nist.gov/PhysRefData/ASD/lines_form.html.
24. Pearse, R. and Gaydon, A., *The Identification of Molecular Spectra,* New York: John Wiley and Sons, 1941.
25. Kortov, V.S., Ermakov, A.E., Zatsepin, A.F., Uĭmin, M.A., et al., Specific features of luminescence properties of nanostructured aluminum oxide, *Phys. Solid State,* 2008, vol. 50, p. 957.

26. Gasenkova, I.V., Mukhurov, N.I., and Vakhiokh, Ya.M., Optical properties of anodized aluminum substrates as the basis for threshold detectors, *Dokl. Beloruss. Gos. Univ. Inf. Radioelektron.,* 2016, no. 2, p. 114.

27. Kacher, I.E., Shuaibov, A.K., Rigan, M.Yu., and Dashchenko, A.I., Optical diagnostics of laser evaporation of $CuInS_2$ polycrystalline compound, *High Temp.,* 2002, vol. 40, no. 6, p. 814.

28. van der Horst, R.M., Verreycken, T., van Veldhuizen, E.M., and Bruggerman, P.J., Time-resolved optical emission spectroscopy of nanosecond pulsed discharges in atmospheric-pressure N_2 and N_2/H_2O mixtures, *J. Phys. D: Appl. Phys.,* 2012, vol. 45, p. 345201. https://doi.org/10.1088/0022-3727/45/34/345201

29. Novikov, G.F. and Gapanovich, M.V., Third-generation Cu–In–Ga–(S, Se)-based solar inverters, *Phys.-Usp.,* 2017, vol. 60, no. 2, p. 161.

30. Mesyats, G.A., Ecton or electron avalanche from metal, *Phys.-Usp.,* 1995, vol. 38, no. 6, p. 567. https://doi.org/10.1070/PU1995v038n06ABEH000089

31. Levko, D. and Raja, L.L., Early stage time evolution of a dense nanosecond microdischarge use in fast switching applications, *Phys. Plasmas,* 2016, vol. 22, p. 123518. https://doi.org/10.1063/1.4939022

32. Gomonai, A.N., Radiative decay of autoionizing np^2-states during dielectronic recombination of Zn^+ and Cd^+ ions, *J. Appl. Spectrosc.*, 2015, vol. 82, no. 1, p. 13.

33. Shuker, R., Binur, Y., and Szoke, A., Studies of afterglows in noble-gas mixtures. A model for energy transfer in He/Xe, *Phys. Rev. A.,* 1975, vol. 12, no. 2, p. 515. https://doi.org/10.1103/PhysRevA.12.515

34. Biberman, L.M., Vorob'ev, V.S., and Yakubov., I.T., *Kinetika neravnovesnoi nizkotemperaturnoi plazmy* (Kinetics of Nonequilibrium Low-Temperature Plasma), Moscow: Nauka, 1982.

35. Strelkov, L.A. and Yankovskii, A.A., Variation of spectral-line intensity during spark discharge, *J. Appl. Spectrosc.,* 1973, vol. 19, no. 4, pp. 1265–1271.

36. Novikov, G.F. and Gapanovich, M.V., Third-generation Cu-In-Ga-(S, Se)-based solar inverters, *Phys.-Usp.,* 2017, vol. 60, no. 2, p. 161. https://doi.org/10.3367/UFNe.2016.06.037827

37. Minya, O.I., Krasilinets', V.M., Shuaibov, O.K., Shevera, I.V., et al., Transmission spectra of copper, aluminum and chalcopyrite-based thin nanostructured films prepared by gas discharge technique, *Nauk. Visn. Uzhhorod Univ. Ser. Fiz.,* 2019, no. 46, p. 84.

38. BOLSIG+ Software. https://nl.lxcat.net/solvers/BOLSIG+/.

39. Shimon, L.L., Influence of autoionization states on the population of energy levels of atoms of the aluminum subgroup, *Nauk. Visn. Uzhhorod Univ. Ser. Fiz.,* 2007, vol. 20, p. 55.

Translated by L. Mosina